Available online at www.sciencedirect.com
ScienceDirect
Thin Solid Films 516 (2008) 8106–8111
www.elsevier.com/locate/tsf

Reconstruction of lattice structure of ion-implanted near-surface regions of $Hg_{1-X}Cd_XTe$ epitaxial layers

A.P. Vlasov [a], O.Yu. Bonchyk [a,*], S.G. Kiyak [a], I.M. Fodchuk [b], R.M. Zaplitnyy [b], T. Kazemirskiy [b], A. Barcz [c], P.S. Zieba [d], Z. Swiatek [d], W. Maziarz [d]

[a] Institute for Applied Problems of Mechanics and Mathematics of NASU, 3-b Naukova Str., 79601, L'viv, Ukraine
[b] Chernivtsi Fedkovich National University, 19 Universitetska Srt., 74012, Chernivtsi, Ukraine
[c] Institute of Physics of Polish Academy of Sciences, 32/46 Al. Lotnikow, 02-668 Warsaw, Poland
[d] Institute of Metallurgy and Materials Science, Polish Academy of Sciences, 25 Reymonta Str., 30-059 Cracow, Poland

Available online 18 April 2008

Abstract

The results of X-ray, SIMS, SEM and AFM studies of near-surface regions of $Hg_{1-X}Cd_XTe$ (111) and (110) structures have been presented. These structures were obtained during annealing in the vapour of main components of ISOVPE $Hg_{1-X}Cd_XTe$ epitaxial layers with the surface implanted with arsenic ions. Berg-Barrett topography method and two-crystal spectrometry technique were exploited. For calculation of depth dependences of deformations and concentrations of dominating defects in the layer's near-surface regions, the Takagi-Taupin equation and generalized dynamic theory of X-ray scattering were used. From experimental SIMS analysis, the distributions of both impurity and main components of $Hg_{1-X}Cd_XTe$ solid solution were determined providing more accurately the deformation profiles in near-surface regions of the structures. SIMS and SEM analyses have given evidence of abrupt gradients of content in the $Hg_{1-X}Cd_XTe$ solid solution, due to small changes of thermodynamical equilibrium conditions of high-temperature annealing in the near-surface regions. These are the cause of formation of a graded-gap structure with strains in the crystal lattice. AFM studies have demonstrated that the morphology of $Hg_{1-X}Cd_XTe$ structures is subjected to the influence of CdTe substrate orientation.

Keywords: Mercury cadmium telluride; X-ray topography; Graded-gap structures

1. Introduction

$Hg_{1-X}Cd_XTe$ narrow gap semiconductor solutions (with molar content $X_{Cd}=0.2$ and 0.3) serve as a basic material for the fabrication of high efficiency detectors of IR radiation in the spectral range of interest (8–12 and 3–5 μm) belonging to the atmospheric transparency window [1]. Modern directions of development of $Hg_{1-X}Cd_XTe$ multiplayer device structures include the 3D band-gap engineering for the fabrication of uncooled photon detectors on their base [2]. The most suitable cover for passivation of the working surface of such detectors is a wide-gap semiconductor with an isotope crystal structure and approximately the same lattice parameters — cadmium telluride CdTe. Thermal treatment of CdTe/$Hg_{1-X}Cd_XTe$ heterostructure causes the formation of a material with gradual distribution of composition which improves the characteristics of passivation cover [3]. This is the consequence of the processes of interdiffusion of the main components of the solid solution. With such a cover at the semiconductor interface, there occurs a redistribution of crystal lattice stresses and a region with special inhomogeneity of band-gap structure is formed. Due to the existence of built-in electric fields, this region greatly influences the diffusion of charged impurities and gives rise to changes in the profile of their distribution [4]. In this paper, we experimentally investigate the factors that cause formation of crystal lattice deformations in the near-surface layers of $Hg_{1-X}Cd_XTe$ graded-gap structures doped with an impurity.

* Corresponding author.
E-mail address: bonchyk@ukr.net (O.Y. Bonchyk).

0040-6090/$ - see front matter © 2008 Elsevier B.V. All rights reserved.
doi:10.1016/j.tsf.2008.04.075

2. Experimental details

We have used n-type $Hg_{1-X}Cd_XTe$ epitaxial layers grown by a modified ISOVPE method of evaporation-condensation-diffusion for these experiments [5]. The layers were grown on CdTe substrates with (111) and (110) crystal orientations. The thickness of these epitaxial layers was ~73 μm, the initial content of Cd atoms at the surface was $X_{Cd}=0.21$ and 0.23, respectively. The impurity source was created by As implantation with the energy $E=100$ keV and the dose $D=1\times10^{15}$ cm^{-2}. The graded-gap structure in the near-surface region of implanted epitaxial layers of $Hg_{1-X}Cd_XTe$ was formed during thermal annealing (at $T\approx600$ °C for 10 min) of the initial structure in Hg and Cd saturated vapours [4]. As shown in [6], this annealing gives rise to the content conversion at the surface of $Hg_{1-X}Cd_XTe$ right up into CdTe. In the obtained graded-gap structures, the diffusion-controlled transfer process of an impurity has been carried out simultaneously under identical annealing regimes.

For X-ray studies of $Hg_{1-X}Cd_XTe$ epitaxial layers, we employed Berg-Barrett topography method using symmetric, unsymmetric and skew asymmetric schemes of obtaining X-ray topograms and the method of two-crystal spectrometry.

Distribution of impurity concentration and composition profile of $Hg_{1-X}Cd_XTe$ epitaxial layers were investigated by mass-spectrometry of secondary ions with a Cameca IMS-6F device. An analysis of impurity and isotope of the main component of CdHgTe (202Hg130Te) was carried out simultaneously. Besides, the mean value of molar content of Cd at the structure surface was determined by X-ray microanalyser Philips CM20. Contactless atomic-force microscopy with a NanoScope-IIIa Dimension 3000™ device was used for analysis of the surface morphology of the $Hg_{1-X}Cd_XTe$ graded-gap structures.

3. Results and discussion

For non-destructing layer-by-layer analysis of structural changes in the near-surface layers, we used the skew-asymmetric scheme of diffraction on reflection with subsequent azimuth scanning around the diffraction vector [7]. Such a diffraction scheme provides wide possibilities of layer-by layer visualization of structural changes in the near-surface crystal's layers, since the change of scanning angle ϕ is connected with the change of extinction depth L_{ext} by the expression:

$$L_{ext}=\frac{\lambda}{C|\chi_h|}\sqrt{\gamma_0|\gamma_h|},\gamma_{0,h}=\pm\sin\theta\cos\psi-\cos\theta\sin\psi\cos\varphi, \quad (1)$$

where γ_0 is the angle of incidence of beam on the crystal surface, γ_0 is the outlet angle, C is the coefficient of polarization, χ_h is the Fourier component of polarizability, θ is the diffraction angle, Ψ is the angle of off-orientation between the incident and reflection crystallographic planes, so that the condition $\Psi-\theta\le1°$, λ should be satisfied, where λ is the X-ray wavelength.

The images of $CuK_{\alpha1}$ and $CuK_{\alpha2}$ reflections in the X-ray topograms of $Hg_{1-X}Cd_XTe$ graded-gap structures with (111) and (110) crystal orientations for (333) and (440) symmetric reflections, respectively, are clearly separated and almost

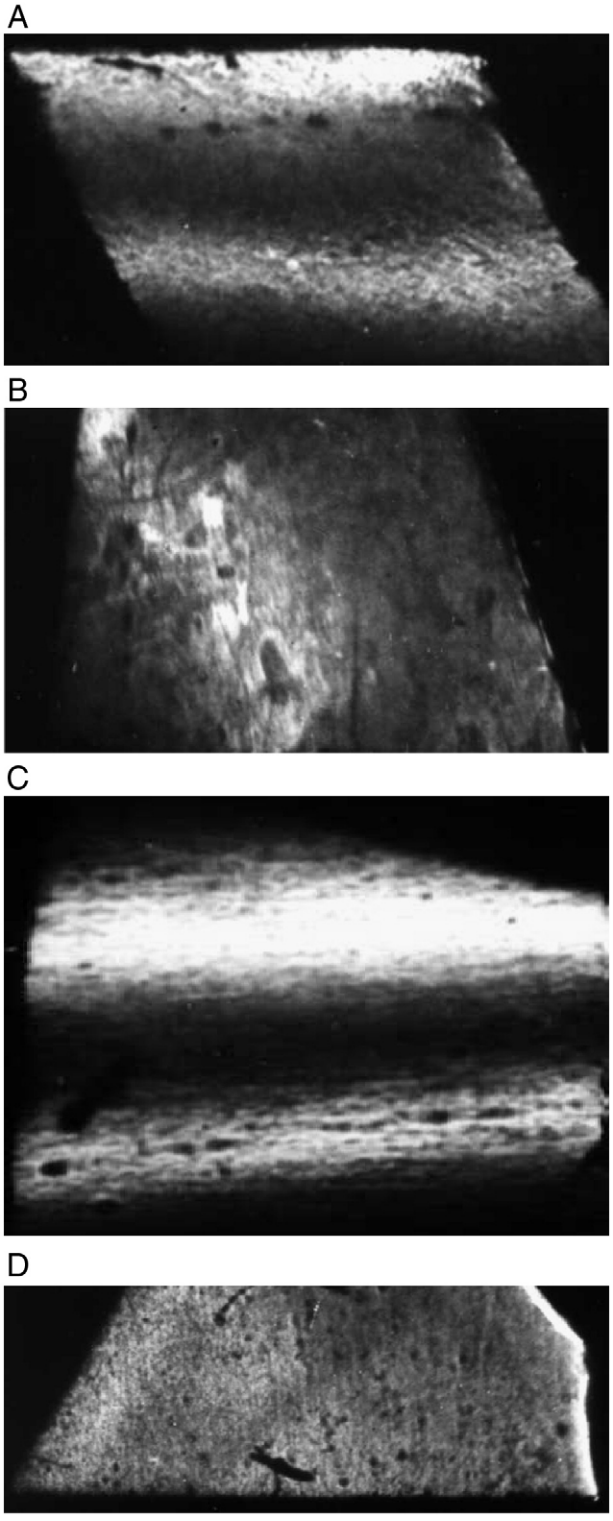

Fig. 1. X-ray topograms of $Hg_{1-X}Cd_XTe$ epitaxial structures ((111) — A, B, (110) — C, D). CuKα-radiation: a) symmetrical reflection (333), b) skew-asymmetrical (511), $L_{ext}=1$ μm; c) symmetrical (440); d) unsymmetrical (511), $L_{ext}=1.2$ μm. Increase 15×.

straight (Fig. 1A and C). More fuzzy and non-uniform images of epitaxial layers are seen in the topograms obtained in the skew-asymmetric and unsymmetric schemes when the depth of penetration of X-rays in the near-surface layers decreases substantially (Fig. 1B and D). For the $Hg_{1-X}Cd_XTe$ (110) epitaxial layer (Fig. 1D), the topographical image is more uniform and has the fine-grained form with inclusion of another phase (telluride and mercury in their nature [8]) and micropores. The surface of $Hg_{1-X}Cd_XTe$ (110) epitaxial structure is more homogeneous and the images show a set of parallel dark lines along the $CuK\alpha_1$ and $CuK\alpha_2$ X-ray reflection (Fig. 1C). The latter indicates that, in the near-surface layers of the structure, a set of misfit dislocations is present, parallel to its surface, which can be caused either by the localization of arsenic ions or by the region of sharp composition gradient in the $Hg_{1-X}Cd_XTe$ solid solution.

Rocking curves (RC) from the fabricated $Hg_{1-X}Cd_XTe$ (111) and (110) graded-gap structures have been obtained using the two-crystal spectrometer (Fig. 2A and B). In order to eliminate the influence of dispersion on the formation of rocking curves,

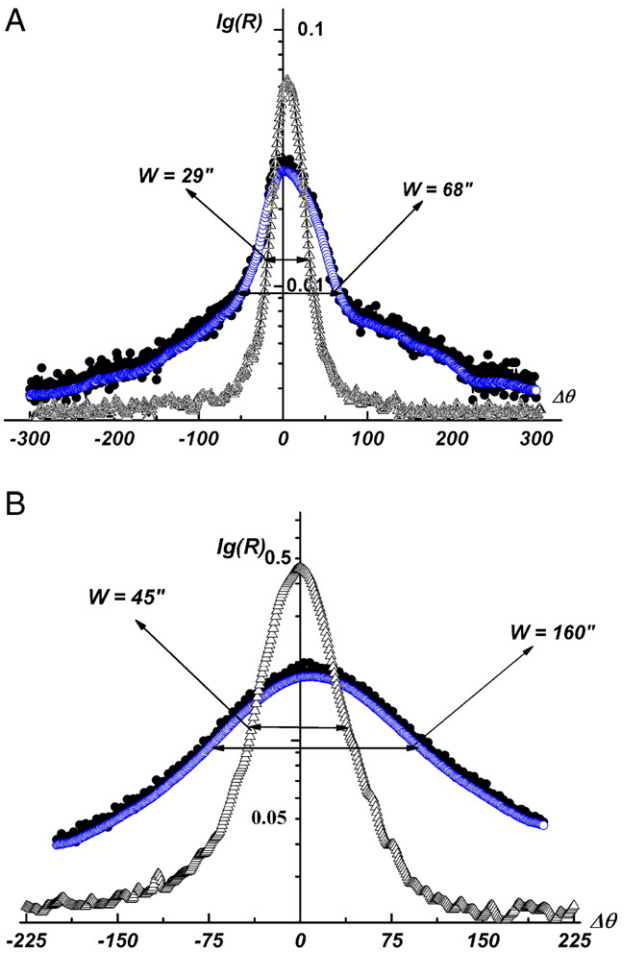

Fig. 2. RC for $Hg_{1-X}Cd_XTe$ epitaxial structures with crystal orientation (111) — (A) ((333) reflection of CuKα-radiation) and (110) — (B) ((220) reflection of CuKα-radiation), R is the coefficient of reflection of X-rays, $\Delta\theta$ is the angle deviation. ● — experimental curve; ○ — theoretical curve; Δ — RC for CdTe standard substrates.

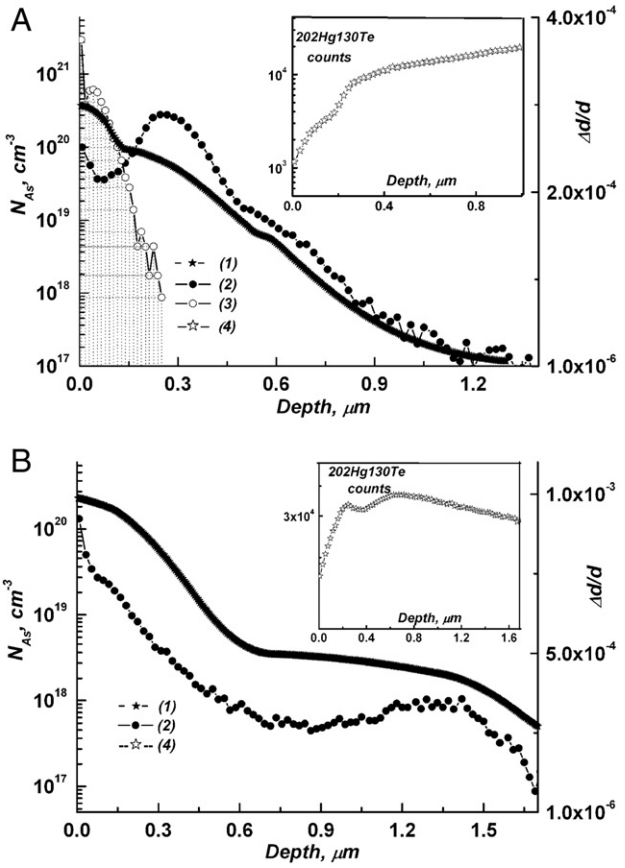

Fig. 3. (A, B) — calculated crystal lattice deformation profiles (1) and experimental SIMS-profiles of As distribution in obtained $Hg_{1-X}Cd_XTe$ epitaxial structures (2) with (111) and (110) crystal orientations, respectively. (A) Shows initial SIMS-profile of As distribution after ion implantation (3). On the insets the profiles of distribution of the number of 202Hg130Te isotope pulses (4) in near-surface regions of studied samples are presented.

we used InSb (333) monochromator for (333) symmetric of CuK_α — radiation and CdTe (220) one for (220) reflection, respectively. As seen in Fig. 2, the RCs have asymmetric form and are characterized by substantial increase in the half-width of RC (W), as well as rather elevated "tails" in comparison with CdTe standard sample. This is caused by a set of defects related to imperfection of $Hg_{1-X}Cd_XTe$ epitaxial layers due to the inheritance of defect structure in the substrates, inhomogeneity of main component distribution over the depth of epitaxial structure after annealing, and the change of crystal perfection of a material due to impurity ion implantation.

Using the magnitudes of angle magnification of half-width of rocking curves, we have estimated the possible density of dislocations [9]: $\approx 10^5$ sm^{-2} for $Hg_{1-X}Cd_XTe$ (111) layers and $\approx 2{\cdot}10^6$ sm^{-2} for $Hg_{1-X}Cd_XTe$ (110) layers.

For determining and defining more accurately the depth profiles of deformations from the rocking curves, we have used the combination of two approaches based on fitting of rocking curves, namely, numerical solution of Takagi's equations [10,11] and the theory developed in [12]. As a first approximation of the depth distribution of deformation, we have chosen the distribution of diffusing As impurity using SIMS analysis data upon number of pulses of 202Hg130Te isotope (Fig. 3).

The maximum value of stresses in the $Hg_{1-X}Cd_XTe$ (111) sample is observed near the surface in the region of abrupt graded-gap structure (≈0.15 μm from the surface). The average value of molar content of solid solution at the sample surface determined with the help of X-ray microanalysis amounts to $X_{Cd} \approx 0.8$, and its largest changes established by SIMS analysis on the number of pulses of 202Hg130Te isotope reach the thickness of up to 0.3 μm (inset of Fig. 3A). In this region, a non-monotonic character of the distribution of diffusing impurity is displayed. This distribution is characterized by the presence of clearly defined maximum and minimum. Such a peculiarity of impurity distribution is caused by the influence of internal built-in electric field in the graded-gap structure on the diffusion of arsenic [4]. Location of the deformation maximum is close to the sample surface when compared with the maximum of concentration of diffusing impurity. The extent of deformation changes is determined mainly by the change of molar content of the near-surface regions of $Hg_{1-X}Cd_XTe$ (111) epitaxial structure (inset of Fig. 3A).

SIMS distribution of arsenic for the $Hg_{1-X}Cd_XTe$ (110) structure (Fig. 3B) substantially differs from the former. One cause of this difference is the process of channeling of impurity ions in the loosely packed lattice [13]. Effect of ion channeling in such a structure increases the depth of penetration of impurity and has no influence on the processes of interdiffusion of the main components in the near-surface layers. As compared with the previous structure, one can not clearly separate the contributions of incorporated impurity and changes of molar content in the stress of crystal lattice on the obtained profiles, however the maximum value of deformation in this sample is greater by the factor of 3. This can be caused by the total stress of the two mentioned factors on the crystal lattice.

In the theory [12,14,15], which the authors referred as a generalized theory of dynamic scattering of X-rays, the reflection coefficient of X-rays from single crystals with homogeneously distributed defects consists of the coherent ($R_{coh}(\Delta\theta)$) and diffusion ($R_{diff}(\Delta\theta)$) components. We have used the results obtained in those papers for the choice of possible types of dominating defects in the near-surface epitaxial layers and their distribution over the depth [16,17]. In our case, the inhomogeneous near-surface layer was divided into thin sub-layers in which the deformation averaged over the set of available defects is constant and the defects are distributed homogeneously [12,16]. Using the kinematic approximation for each such layer we obtain

$$R(\Delta\theta) = R_{coh}(\Delta\theta) + R_{diff}(\Delta\theta) = |\xi|\left(L - \sqrt{L^2-1}\right) + \sum_{j=1}^{M} a_j \mu_{DS,j} t_j / \gamma_0 \quad (2)$$

where L is the parameter which takes into account the absorption of strong Bragg waves via the processes of non-elastic scattering on defects and additional absorption of these waves due to diffuse scattering on defects, ξ is the coefficient which takes into account the dispersion correction for χ_H, a_j is the absorption coefficient of the incident wave along the thickness of the j-th layer, t is the thickness of the crystal, γ_0 is the dispersion cosine of the wave vector of incident wave.

The static factor of Debye-Waller L_H and the absorption coefficient μ_{DS} present the corresponding superposition over all types of defects due to diffuse scattering at defects in the j-th layer.

They can be described by expressions

$$L_H = \sum_{\alpha} L_H^{\alpha}, \quad \mu_{DS} = \sum_{\alpha} \mu_{DS}^{\alpha}, \quad (3)$$

where α numbers the defect type. The factor L_H in Eq. (3) is related to the characteristics of dominating defects by the relations.

$L_H^D \approx 0.5 c v_0^{-1} R_0^3 (H \cdot b)^{3/2}$ — for dislocation loops;
$L_H^K \approx 0.5 c n_0 \eta^2 (1 - \eta^2/100)$: $(\eta^2 << 10)$;
$L_H \approx c n_0 \eta^{3/2}$: $(\eta^2 >> 10)$ — for spherical and disk-like clusters.

Where c is the concentration of the respective type of defects, v_0 is the number of atoms in cubic lattice unit of the matrix, R_0 is the actual radius of defect, H is the vector of reversed lattice, b is the Burgers vector of dislocation loop, n_0 is the number of lattice units that are substituted by cluster, $\eta = \alpha_0 n_0^{1/3} H a_0/(2\pi)$, $\alpha_0 = \Gamma \varepsilon R_0^2 h_p/2$, h_p is the cluster thickness, a is the lattice constant, ε is the deformation at the interface of cluster, $\Gamma = (1+\nu)(1-\nu)^{-1}/3$, ν is the Poisson's coefficient.

The coefficient of absorption μ_{DS} that arises as a consequence of diffuse scattering in the j-th layer is determined by the relation [12]:

$$\mu_{DS,j}^{\alpha}(k_0) = c_{\alpha}(z_j) C^2 (E_j)^2 m_0 J_j^{\alpha}(k_0), m_0 = \frac{\pi v_c}{4} (H|\chi_{rH}|/\lambda)^2, E = \exp(-L_H), \quad (4)$$

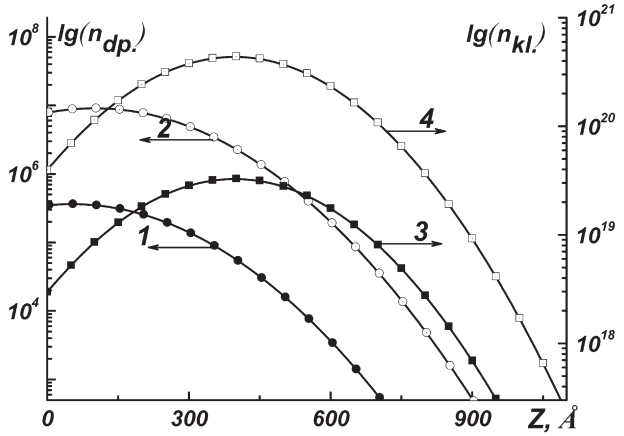

Fig. 4. Concentration profiles of defects 1, 2 — distribution of concentration of dislocation loops (n_{dp}); 3, 4 — clusters (n_{kl}). (Curves 1, 3 for $Hg_{1-X}Cd_XTe$ (111), 2, 4 — for $Hg_{1-X}Cd_XTe$ (110)).

where: $c_\alpha(z)=c_{\alpha,m}f_{c,\alpha}(z)$ is the distribution of concentration of defects of type α in the disturbed layer, $c_{\alpha,m}$ is the maximum magnitude of concentration of defects in the disturbed layer, $f_{c,\alpha}$ (z) is an arbitrary (normalized on unity) function of distribution of defect concentration in the disturbed layer, C is the polarizability factor, v_c is the number of atoms in the cubic cell of the matrix, H is the absolute value of the vector of reciprocal lattice, χ_{rH} is the Fourier components of polarizability, λ is the wavelength, $J_j^\alpha(k_0)$ is the normalized coefficient of absorption via diffuse scattering.

On the basis of the above mentioned changes of defect structure in the near-surface layers of $Hg_{1-X}Cd_XTe$, we suggest setting up, during formation of the graded-gap structure, of a set of defects: Frenkel's pairs, complexes with point defects — cluster formation and dislocation loops.

In order to calculate diffraction curves using relation (2), initial depth dependencies of concentrations $n(z)$ and defect radii $R(\alpha)$ in disturbed near-surface layers were specified by asymmetrical Gaussians Eq. (5). Initial deformation profile was calculated by solving Takagi–Taupin equations [10,11].

$$n(z) = n_{\max}(\alpha)f(z), R(\alpha) = R_{\max}(\alpha)f(z), \tag{5}$$

where: $R_{\max.}(\alpha)$ is the maximum value of radius of α-type defects; $n_{\max.}$ is the maximum value of concentration of defects in the disturbed layer.

$$f(z) = \begin{cases} \exp\left[-(z-Z)^2/\sigma_1\right], \text{if} \quad 0<z<Z \\ \exp\left[-(z-Z)^2/\sigma_2\right], \text{if} \quad z\geq Z \end{cases} \tag{6}$$

where z is the distance counted off from the surface inside crystal, Z is the point of joining the Gaussians, σ_1, σ_2 are the parameters of Gaussians that characterize their half-width.

Calculation of diffraction curves with the help of Eqs. (2, 5, 6), allows one to obtain the concentration profiles (Fig. 4) of dominating types of defects and make the corrections for the depth profiles of deformations in the disturbed layers.

Atomic-force microscopy study shows insignificant differences in the morphologies of the initial surface and that modified by implantation and annealing (Fig. 5). The surface of each region contains a certain number of various defects and inclusions. Initial (before the implantation) regions of the studied structures are characterized by roughnesses and steps on the surface of the sample. Their concentration decreases and the surface becomes more homogeneous after implantation and annealing and the surface becomes more uniform due to relaxation of elastic deformations just in the near-surface region of epitaxial layers, which is confirmed by the calculated profiles of the concentrations of defects and deformation profiles. The maximum value of roughness $R_a=0.874$ nm (average deviation of heights from the mean plane of the surface relief) is characteristic of the non-implanted region. For the implanted one, the roughness amounts to $R_a=0.651$ nm.

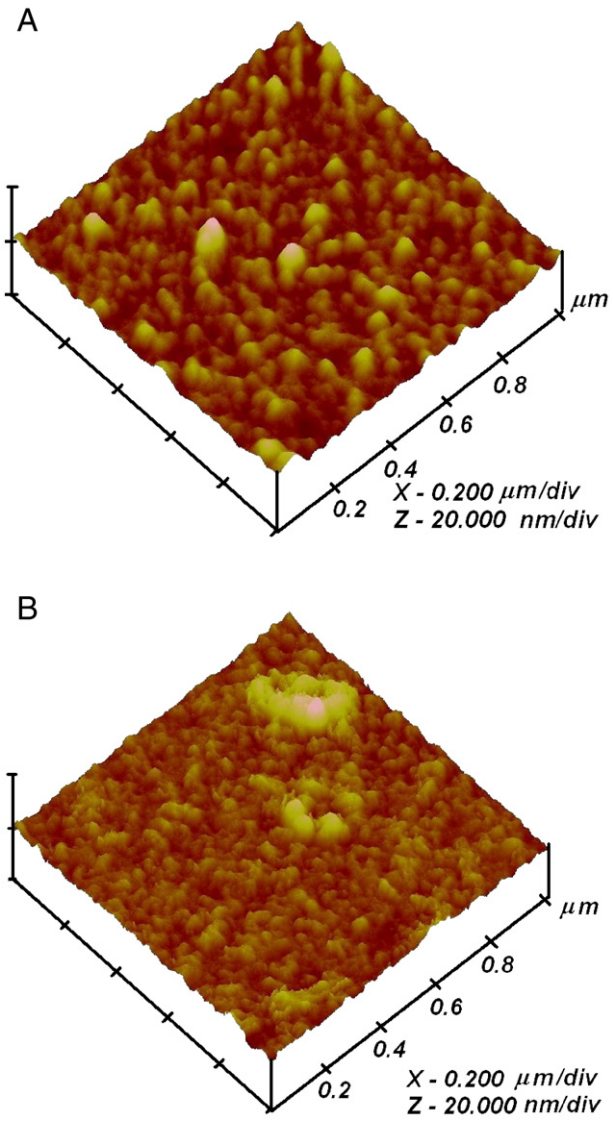

Fig. 5. AFM topograms of HgCdTe(110) epitaxial layer before (A) and after sequential processes of As implantation and annealing (B).

4. Conclusions

- Maximum deformation of crystal lattice is caused by the presence of a graded-gap structure in the near-surface regions of modified $Hg_{1-X}Cd_XTe$ epitaxial layers.
- Deformations of crystal lattice of $Hg_{1-X}Cd_XTe$ caused by the presence of a graded-gap region give rise to larger stresses in comparison with those connected with implanted impurity atoms with concentration $N_{As}\approx 1\times10^{17}\div5\times10^{18}$ cm^{-3}.

References

[1] A. Rogalski, Rep. Prog. Phys. 68 (2005) 2267.
[2] J. Piotrowski, Opto-Electron. Rev. 12 (2004) 111.
[3] R. Pal, A. Malik, V. Srivastav, B.L. Sharma, V. Dhar, B. Sreedhar, H.P. Vyas, J. Electron. Mater. 35 (2006) 1793.
[4] A.P. Vlasov, B.S. Sokolovskii, L.S. Monastyrskii, O.Yu. Bonchyk, A. Barcz, Thin Solid Films 459 (2004) 28.
[5] V.G. Savitsky, O.P. Storchun, Thin Solid Films 317 (1998) 105.
[6] S.Y. An, J.S. Kim, D.W. Seo, S.H. Suh, J. Electron. Mater. 31 (2002) 683.

[7] I.M. Fodchuk, S.A. Kshevetskiy, Metallofizika (Ukr. Phys.) 14 (1992) 57.
[8] A. Vlasov, A. Bonchyk, I. Fodchuk, and P. Zaplitnyi, Collected Scientific Papers of G.V. Karpenko Physico-Mechanical Institute of Academy of Sciences of Ukraine, Issue 9: Physical methods and means of monitoring of environment, materials and products, Kyiv, 2004, p. 156.
[9] D.K. Bowen, B.K. Tanner, High Resolution X-ray Diffractometry and Topography, Taylor & Fracis, London, 1998, p. 264.
[10] R.N. Kyutt, P.V. Petrashen, L.M. Sorokin, Phys. Stat. Sol.(a) 60 (1980) 381.
[11] V.G. Kohn, M.V. Kovalchuk, R.M. Imamov, E.F. Lobanovich, Phys. Stat. Sol. (a) 64 (1981) 435.
[12] S.I. Olikhovskii, V.B. Molodkin, E.N. Kislovskii, et al., Phys. Stat. Sol. (b) 231 (2002) 199.
[13] R.G. Wilson, J. Appl. Phys. 63 (1988) 5302.
[14] P.H. Dederichs, Solid State Phys. 27 (1972) 135.
[15] V. Holy, U. Pietsch, T. Baumbach, Higt-Resolution X-Ray Skattering from Thin Films and Multilayers, Springer-Verlag, Berlin, 1999, p. 253.
[16] I. Fodchuk, R. Zaplitnyy, T. Kazemirskiy, Z. Swiatek, Phys. Stat. Sol. (a) 204 (2007) 2714.
[17] A.P. Vlasov, O.Yu. Bonchyk, I.M. Fodchuk, R.A. Zaplitnyy, A. Barcz and Z.T. Swiatek, Semiconductor Physics, Quantum Electronics & Optoelectronics 9 (2006) 36.